Supporting Information

Oxygen Vacancy Engineering and Redox Coupling-driven Enhancement of Extended Wavelength Light Absorption and Energy Storage in $Ca(OH)_2$–$Sr_{0.4}Co_{2.6}O_4$ via Photothermal Dehydration

Lin Zhu,[1] Rui-Min Hao,[1] Ti-Jian Du,[2] Cheng-Hui Liu,[3] Zhi-Bin Xu,[1] and Qin-Pei Wu*[1]

[1]School of Chemistry and Chemical Engineering, Beijing Institute of Technology, Beijing, 102488, China
[2]Yantai Valiant Pharmaceutical Co., Ltd. 60 Taiyuan Rd, Dajijia Industrial Park, YEDA Yantai, Shandong, China
[3]School of Material Science and Engineering, Beijing Institute of Technology, Beijing, 102488, China

E-mail address: qpwu@bit.edu.cn

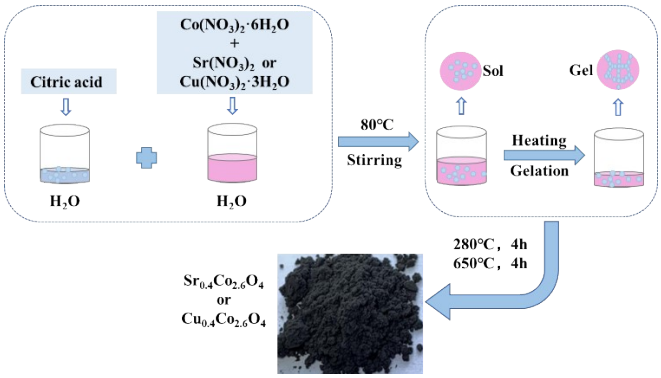

Figure S1. Graphical scheme for the preparation of $M_xCo_{3-x}O_4$.

1. Photothermal conversion efficiency of CaCoSr-15

To evaluate the photothermal conversion efficiency of $Sr_{0.4}Co_{2.6}O_4$ or $Ca(OH)_2$–15-wt% $Sr_{0.4}Co_{2.6}O_4$ (CaCoSr-15), 200 μL of the CaCoSr-15 aqueous solutions was exposed to the irradiation under 5.1 $W \cdot cm^{-2}$ 808 nm or 1064 nm laser for 2 min. Subsequently, the solutions cooled down naturally. The temperature changes were recorded by an infrared thermal imaging

camera every 30 s. The photothermal conversion efficiency (η) can be calculated according to the Eq (S1).

$$\eta_{trans} = \frac{hS(T_{max} - T_{surr}) - Q_{dis}}{I(1 - 10^{-A})} \quad \text{(S1)}$$

$$\tau_s = \frac{(m_D c_D)}{hs} \quad \text{(S2)}$$

Here, the maximum temperature of $Sr_{0.4}Co_{2.6}O_4$ or CaCoSr-15 solution and the ambient temperature are denoted by T_{max} and T_{surr}, respectively. The light intensity and the absorption value of the material at wavelength λ (1064 nm) are denoted as I (5.1 W·cm^{-2}) and A (1.56), respectively. Here h (W·cm^{-2} K^{-1}) means heat-transfer coefficient, s (cm^2) represents the surface area of the container. Q_{dis} is heat loss from light absorbed by the container, and it is calculated to be approximately equal to 0 mW.

The τ_s is the sample system time constant, m_D and c_D are the mass (0.2 g) and heat capacity (4.2 J/g) of the solvent, respectively (Eq S2).

Thus, according to calculating, the heat conversion efficiency (η) of the sample under 1064 nm laser is derived, respectively. The mean η is calculated.

The photothermal conversion efficiencies of $Sr_{0.4}Co_{2.6}O_4$, CaCoSr-15 and $Ca(OH)_2$ were measured to be 86.2%, 83.6%, and 1.3%, respectively.

2. Thermal-storage kinetics of $Ca(OH)_2$–$Sr_{0.4}Co_{2.6}O_4$

The kinetics equation for solid–gas reactions:

$$\frac{d\alpha}{dT} = \frac{1}{\beta} k(T) f(\alpha) \quad \text{(S3)}$$

$$\frac{d\alpha}{dT} = \frac{A}{\beta} \exp\left(-\frac{E}{RT}\right) f(\alpha) \quad \text{(S4)}$$

where α is a conversion that can be calculated with equation (Eq S3 and S4), A/s^{-1} is the pre-exponential factor, E/(kJ/mol) is the activation energy, β/(K/min) is the heating rate, T/K is the temperature, R/(J/(mol·K)) is the ideal gas molar constant, and $f(\alpha)$ is the dehydration reaction's

kinetics mechanism function.

The Coats–Redfern (C–R) integral method can be expressed as:

$$\ln\left[\frac{G(\alpha)}{T^2}\right]=\ln\left(\frac{AR}{\beta E}\right)-\frac{E}{RT} \quad \text{(S5)}$$

The Archar–Brindley–Sharp–Wendworth (ABSW) differential equation can be described as:

$$\ln\left[\frac{d\alpha}{f(\alpha)dT}\right]=\ln\left(\frac{A}{\beta}\right)-\frac{E}{RT} \quad \text{(S6)}$$

$$\frac{d\alpha}{dT}=\frac{A}{\beta}\exp\left(-\frac{E}{RT}\right)f(\alpha) \quad \text{(S7)}$$

Table S1 Integral and differential forms of gas-solid reaction mechanism models

Kinetic model	Symbol	$g(\alpha)$	$f(\alpha)$
Arami-Erofeev (n=1)	A1	-ln(1-α)	1-α
Arami-Erofeev	A1.5	$[-\ln(1-\alpha)]^{2/3}$	$3/2(1-\alpha)[-\ln(1-\alpha)]^{1/3}$
Arami-Erofeev	A2	$[-\ln(1-\alpha)]^{1/2}$	$2(1-\alpha)[-\ln(1-\alpha)]^{1/2}$
Arami-Erofeev	A3	$[-\ln(1-\alpha)]^{1/3}$	$3(1-\alpha)[-\ln(1-\alpha)]^{2/3}$
1 dimensional diffusion	D1	α^2	$\alpha^{-1}/2$
2 dimensional diffusion	D2	$(1-\alpha)\ln(1-\alpha)+\alpha$	$[-\ln(1-\alpha)]^{-1}$
Contracting cylinder	R2	$1-(1-\alpha)^{1/2}$	$2(1-\alpha)^{1/2}$
Contracting sphere	R3	$1-(1-\alpha)^{1/3}$	$3(1-\alpha)^{2/3}$

Table S2 Average Rs values for linear fits of C-R and ABSW methods related to bare $Ca(OH)_2$ and $Ca(OH)_2$+15 wt% $Sr_{0.4}Co_{2.6}O_4$

Rs	model					
	R2	R3	F1	D1	D2	A2
Rs ($Ca(OH)_2$)	0.9974	0.9957	0.9955	0.9967	0.9963	0.9951
Rs (CaCoSr-15)	0.9958	0.9908	0.9918	0.9938	0.9918	0.9913

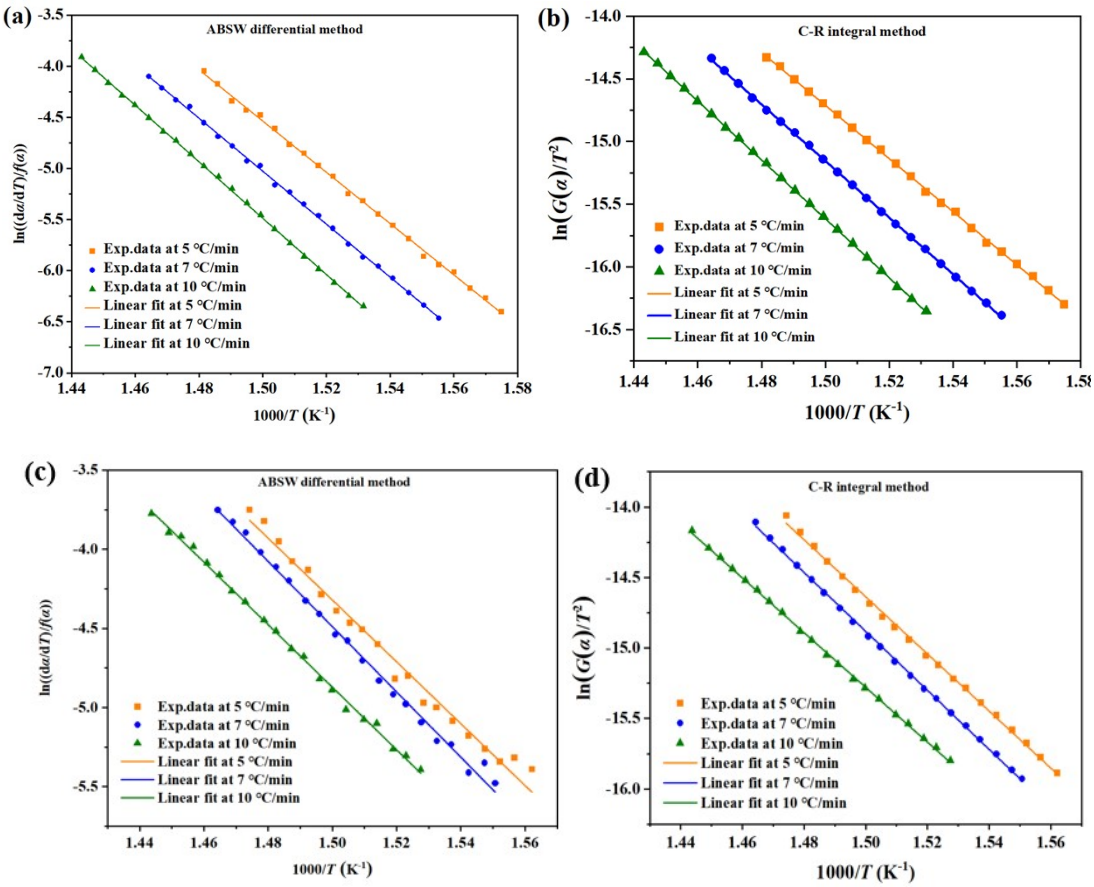

Figure S2 (a) and (b) Linear fitting results of the ABSW differential and C-R integral methods for the dehydration of pure $Ca(OH)_2$, in term of model R2. (c) and (d) Linear fitting results of the ABSW differential and C-R integral methods for the dehydration of $Ca(OH)_2$+15 wt% $Sr_{0.4}Co_{2.6}O_4$, in term of model R2.

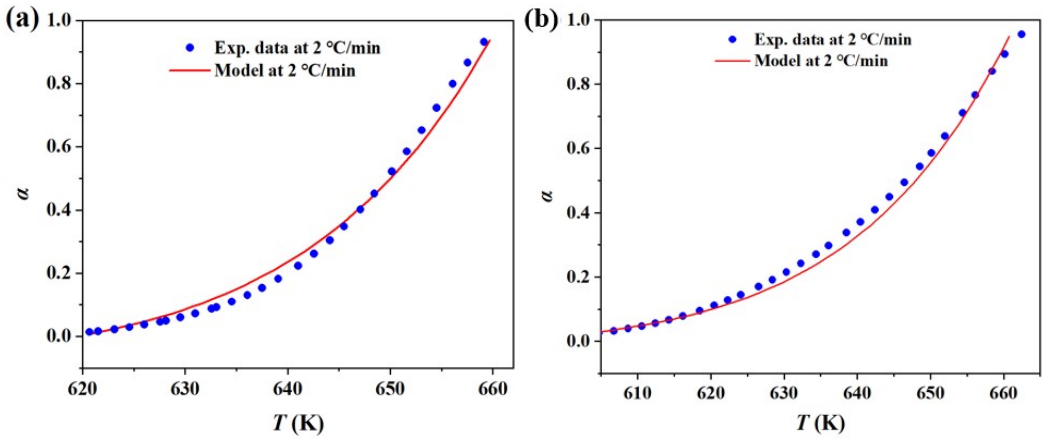

Figure S3. Comparison between the model-calculated data and thermogravimetric analysis

(TGA) results for the dehydration of (a) pure $Ca(OH)_2$ and (b) $Ca(OH)_2$–15 wt% $Sr_{0.4}Co_{2.6}O_4$ composite.

3. Van der Pauw method for measuring the electrical conductivity

Principle: Four electrodes are placed on the surface of a solid sample. A direct current (I) is passed through the two outer electrodes, while the two inner electrodes are used to measure the potential difference (V). The resistance (R) of the sample is calculated using Ohm's law (R = V/I), and the electrical conductivity (σ) is then determined based on the relationship between conductivity and resistance (σ = L/(RA)), where σ is the conductivity, L is the distance between the electrodes, and A is the cross-sectional area of the sample. The Hall coefficient, charge carrier density, electrical conductivity, resistivity, and Hall mobility can be derived from equations S8 to S13.

$$R_H = t \bullet V_H / (I \bullet B) \qquad \text{(S8)}$$

R_H, Hall coefficient (cm^3/C); V_H, Hall voltage (V); t, sample thickness (cm); I, working current (A); B, magnetic intensity (T).

$$n = 1/(R_H \bullet e) \qquad \text{(S9)}$$

n, charge carrier density (cm^{-3}); R_H, Hall coefficient (cm^3/C); e = 1.6×10^{-19} C

$$\sigma = nq\mu_n + nq\mu_p \qquad \text{(S10)}$$

σ, the electrical conductivity (S/cm); n, charge carrier density; q, the charge of charge carriers; μ_n, the electron mobility ($cm^2/(V\cdot s)$); μ_p, the hole mobility.

$$\rho = (\pi \cdot t/\ln 2) \cdot (R_a + R_b)/2 \cdot f(R_a / R_b) \qquad \text{(S11)}$$

$$\rho = 1/\sigma \qquad \text{(S12)}$$

ρ, resistivity ($\Omega\cdot$cm); t, sample thickness (cm); σ, the electrical conductivity (S/cm); R_a and R_b, resistance

value (Ω).

$\mu_H = R_H/\rho$ (S13)

μ_H, Hall mobility ($cm^2/V \cdot s$); R_H, Hall coefficient (cm^3/C); ρ, resistivity ($\Omega \cdot cm$).

Procedure: First, the solid sample is processed into a regular shape, such as a rectangular prism, to ensure uniform current distribution. The four electrodes are evenly mounted on the sample, ensuring good electrical contact between the electrodes and the sample. A stable direct current is applied ($I = 10^{-6}$ A), and the potential difference is measured and recorded under a magnetic field with 0.5-T intensity. The conductivity, Hall coefficient, mobility, and charge carrier density are then calculated using the above formulas.

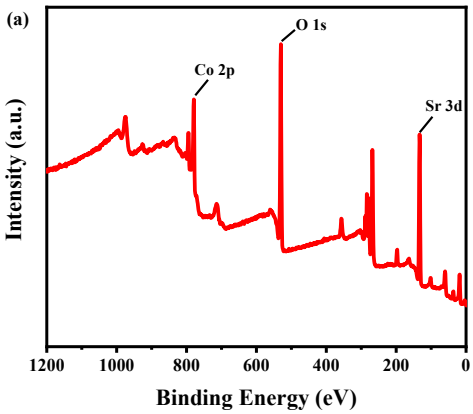

Figure S4. Elemental survey spectrum of X-ray photoelectron spectroscopy spectra for $Sr_{0.4}Co_{2.6}O_4$.

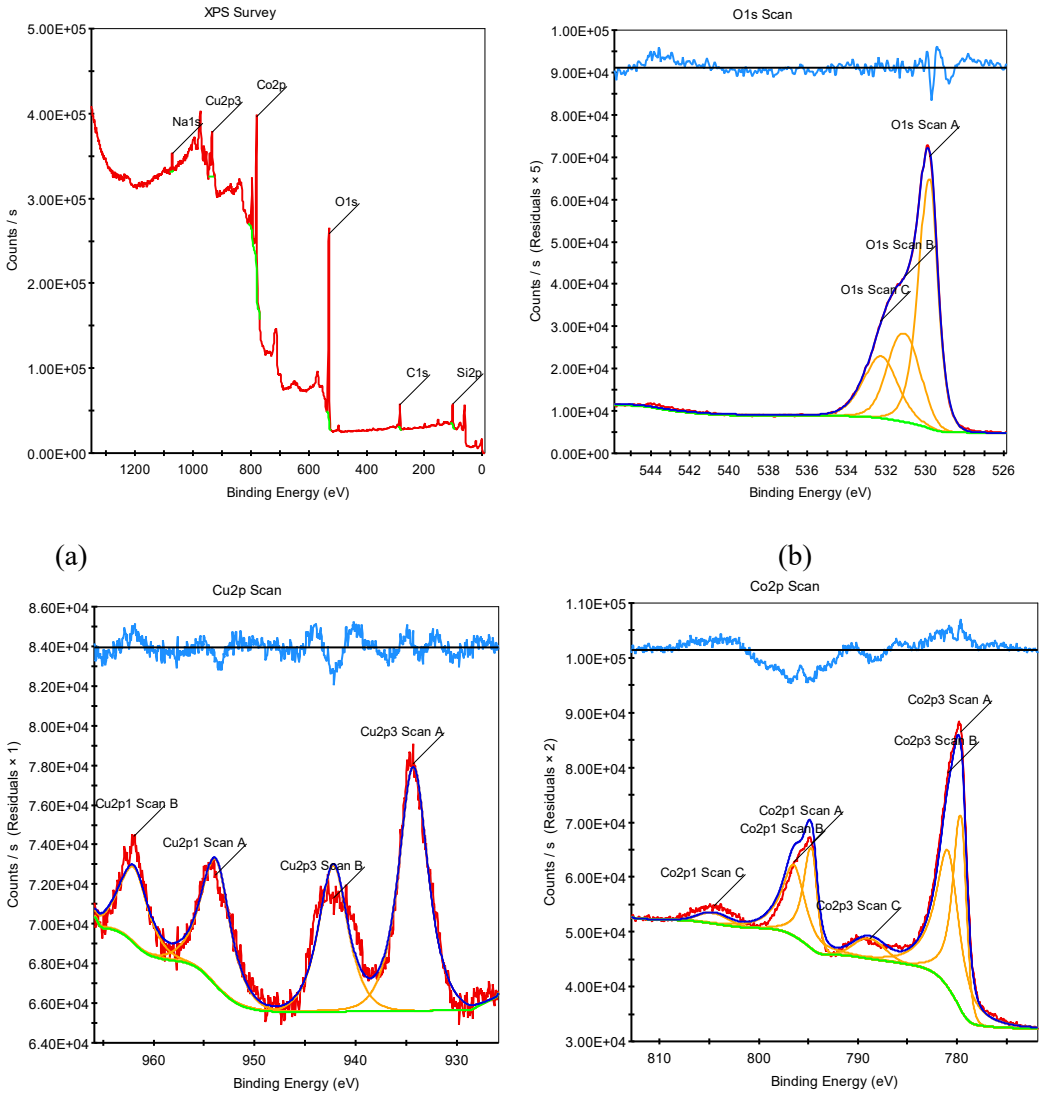

Figure S5. X-ray photoelectron spectroscopy spectra of $Cu_{0.4}Co_{2.6}O_4$. (a) Elemental survey spectrum of $Cu_{0.4}Co_{2.6}O_4$. (b) Deconvoluted spectrum of O 1s for $Cu_{0.4}Co_{2.6}O_4$. (c) Deconvoluted spectrum of Cu 2p for $Cu_{0.4}Co_{2.6}O_4$. (d) Deconvoluted spectrum of Co 2p for $Cu_{0.4}Co_{2.6}O_4$.

Table S3. BE values and the area ratio of BE peaks of O 1s for $Cu_{0.4}Co_{2.6}O_4$ XPS spectra

O 1s BE value	area CPS.ev	Area ratio
529.77 eV	78663.67	0.50
531.02 eV	45009.22	0.28
532.27 eV	35034.19	0.22

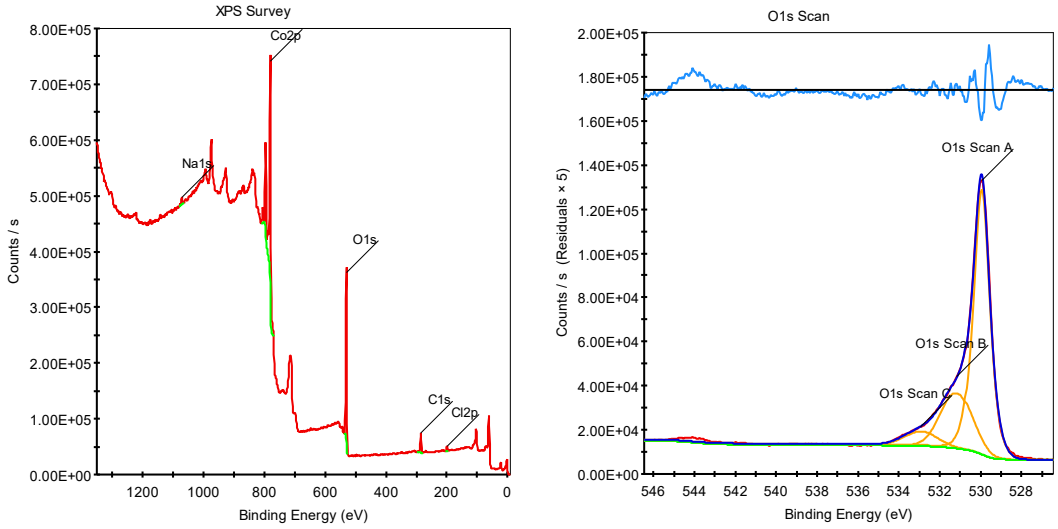

(a) (b)

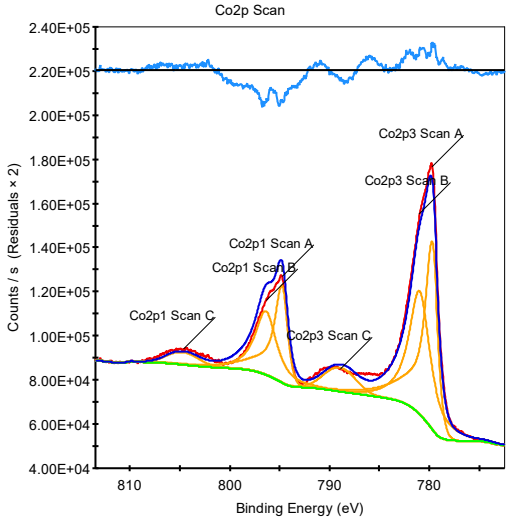

(c)

Figure S6. X-ray photoelectron spectroscopy spectra of Co_3O_4. (a) Elemental survey spectrum of Co_3O_4. (b) Deconvoluted O 1s spectrum of Co_3O_4. (c) Deconvoluted Co 2p spectrum of Co_3O_4.

Table S4. BE values and the area ratio of BE peaks of O 1s for Co_3O_4 XPS spectra

O 1s BE value	area CPS. ev	area ratio
529.96 eV	134896.17	0.68
531.16 eV	49314.75	0.25
532.93 eV	14323.63	0.07

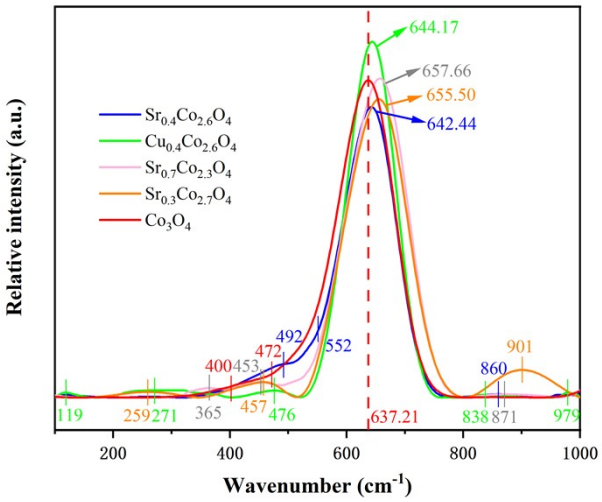

Figure S7. Raman spectra of as-prepared Co_3O_4, $Cu_{0.4}Co_{2.6}O_4$, $Sr_{0.3}Co_{2.7}O_4$, and $Sr_{0.7}Co_{2.3}O_4$.

Table S5 Raman bands of Co_3O_4, $Cu_{0.4}Co_{2.6}O_4$, $Sr_{0.3}Co_{2.7}O_4$, and $Sr_{0.7}Co_{2.3}O_4$

	A_{1g} (cm^{-1})	F_{2g} (cm^{-1})	E_g (cm^{-1})
Co_3O_4	651	615, 528	472
$Sr_{0.4}Co_{2.6}O_4$	663	621, 499	–
$Cu_{0.4}Co_{2.6}O_4$	642	286,119	470
$Sr_{0.7}Co_{2.3}O_4$	653	496	458
$Sr_{0.3}Co_{2.7}O_4$	652	243	451

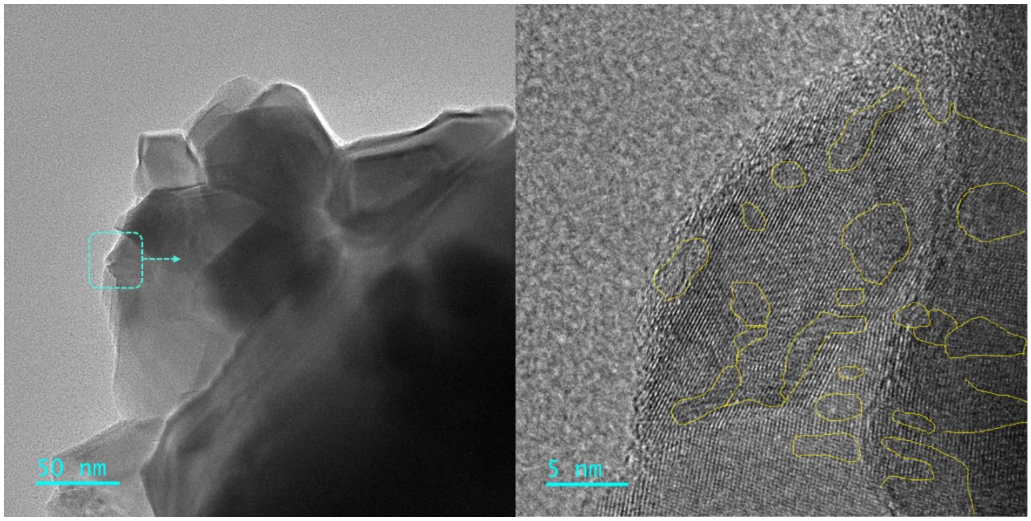

Figure S8. TEM image and HRTEM image of $Sr_{0.4}Co_{2.6}O_4$ and oxygen vacancies marked by yellow lines.

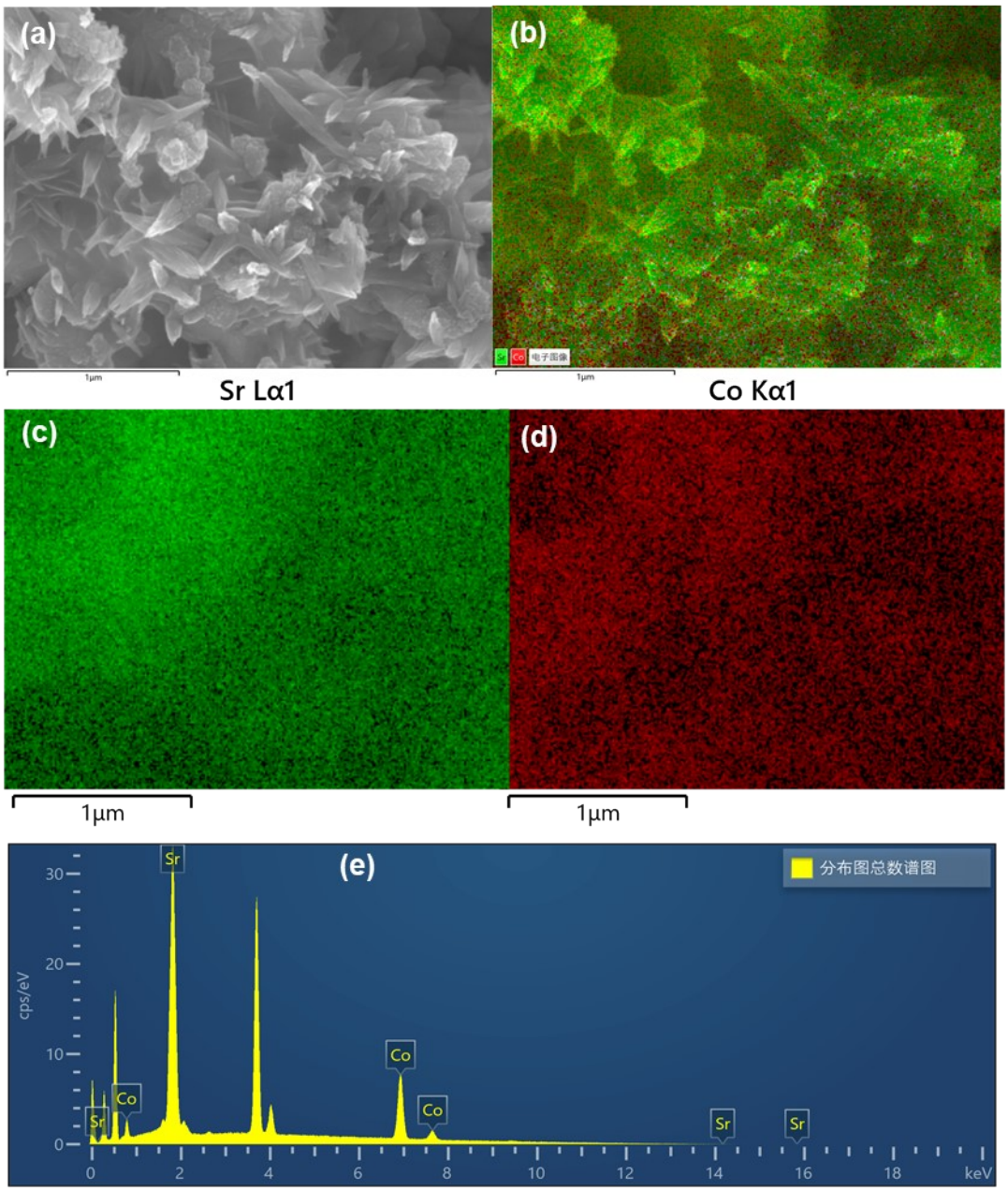

Figure S9 (a) SEM image of $Ca(OH)_2$–15 wt% $Sr_{0.4}Co_{2.6}O_4$ composite. (b) Elemental mapping of the SEM image of $Ca(OH)_2$–15 wt% $Sr_{0.4}Co_{2.6}O_4$ composite. (c) Elemental mapping of the SEM image of $Ca(OH)_2$–15 wt% $Sr_{0.4}Co_{2.6}O_4$ composite for Sr. (d) Elemental mapping of the SEM image of $Ca(OH)_2$–15 wt% $Sr_{0.4}Co_{2.6}O_4$ composite for Co. (b) EDS results of $Ca(OH)_2$–15 wt% $Sr_{0.4}Co_{2.6}O_4$ composite.

Table S6 Elemental contents of $Ca(OH)_2$–15 wt% $Sr_{0.4}Co_{2.6}O_4$ shown in the EDS spectrum

Element	Atom%	Mass%
Co K	86.87	81.65
Sr K	13.13	18.35

Table S7. Photothermal conversion efficiency and photoluminescence intensity of materials

	Co_3O_4	$Cu_{0.4}Co_{2.6}O_4$	$Sr_{0.4}Co_{2.6}O_4$
PL intensity (a.u.)[a]	1.26	1.12	0.84
photothermal efficiency	47.7%	78.3%	86.2%

[a]The average PL intensity in the wavelength range of 414–482 nm.